Lab on a Chip

PAPER

View Article Online
View Journal | View Issue

Cite this: *Lab Chip*, 2025, **25**, 4081

Harnessing intrinsic biophysical cellular properties for identification of algae and cyanobacteria *via* impedance spectroscopy†

Ruben Van den Eeckhoudt, *[a] Naras R. H. Rao, ‡[b] Koenraad Muylaert,[b] Filip Tavernier,[c] Michael Kraft[a] and Irene Taurino[ad]

Received 18th April 2025,
Accepted 27th June 2025

DOI: 10.1039/d5lc00372e

rsc.li/loc

Harmful and nuisance-causing algal blooms, driven by global climatic shifts and eutrophication, present escalating risks to water security, public health, and ecosystems. Effective management of these blooms requires rapid and precise identification of cells to implement targeted intervention. Yet, existing methods are time-intensive, requiring specialized personnel and equipment. Here, we show that *Chlorella vulgaris* (green algae) and *Microcystis aeruginosa* (cyanobacteria), two dominant freshwater species globally, can be differentiated with single-cell resolution by broadband impedance spectroscopy due to the intrinsic differing biophysical character of cyanobacterial and green algal cells. Using a custom microfluidic chip with gold microelectrodes, single cells were trapped via positive dielectrophoresis and analyzed by electrical impedance spectroscopy. We show that the distinct impedance profile of *Microcystis* arises due to the presence of gas vacuoles—non-conductive air pockets, that are absent in *Chlorella*. COMSOL-based simulations confirmed that these vacuoles lower cytoplasmic conductivity and thus, can be used to discriminate species. This label-free approach paves the way for cost-effective, scalable, on-site detection of algae and cyanobacteria, offering a solution to safeguard freshwater resources and preserve global biodiversity.

Introduction

Background

Over the past decades, many lakes, reservoirs and ponds around the world have experienced elevated eutrophication.[1,2] Eutrophication is associated with a rapid increase in the population of algal and cyanobacterial cells, often referred to as nuisance and harmful algal blooms. In addition to eutrophication, climate change is also expected to increase the frequency and intensity of these blooms because algae thrive in warm waters.[3] These algal blooms can be dominated by different groups of algae, including green algae, cyanobacteria (blue-green algae), and diatoms. Generally, green algae and diatoms are problematic because they can create a hypoxic environment for aquatic life, clog waterways and limit the penetration of light into the water, thus impacting the ecosystem. Cyanobacteria pose similar problems as green algae and diatom, but in addition to that they can be harmful as they can release toxins that are detrimental to human and animal life.[4] Moreover, cyanobacteria can generate undesirable taste and odor compounds which interfere with drinking water production.[3,5] Consequently, algal bloom management is deemed essential by authorities and water managers to ensure that aquatic ecosystem health is preserved and can be safely used for recreation, irrigation, and drinking water production.

As these blooms are caused by excessive nutrients, long-term management of blooms can only be achieved by a reduction of nutrient inputs in the affected ecosystem.[6] However, reduction of external nutrient inputs is rarely sufficient to prevent future blooms as these blooms may be sustained for many years by nutrients that have accumulated in the sediments of the water bodies (internal eutrophication[7]). Thus, immediate bloom management strategies are often required. Here, the first step is to correctly identify the type of cells (*e.g.*, green algae, cyanobacteria) as strategies need to be tailored accordingly. While algicides such as bleach or copper sulphate can be dosed to kill green algae and diatoms by cell disruption, they can be detrimental when treating cyanobacteria as cell disruption causes the release of toxins from the cells and an increase in free toxin concentrations in the water.[8] Thus, it is important to correctly identify the type of cells so that appropriate control strategies can be employed.

[a] *Micro- and Nanosystems (MNS), Department of Electrical Engineering (ESAT), KU Leuven, Leuven, Belgium. E-mail: ruben.vandeneeckhoudt@kuleuven.be*
[b] *Laboratory of Aquatic Biology, KU Leuven Kulak, Kortrijk 8500, Belgium*
[c] *MICAS, Department of Electrical Engineering (ESAT), KU Leuven, Leuven, Belgium*
[d] *Semiconductor Physics, Department of Physics and Astronomy, KU Leuven, Leuven, Belgium*

† Electronic supplementary information (ESI) available. See DOI: https://doi.org/10.1039/d5lc00372e

‡ Present address: School of Chemical Engineering, University of New South Wales (UNSW), Sydney, Australia.

Several methods currently exist for the identification of cells. Typically, these encompass microscopical detection methods such as cell imaging and enumeration *via* light microscopy, flow cytometry with chemical labelling, digital flow imaging, and molecular techniques that include DNA and RNA analysis for taxonomic identification.[9–11] They require specialized protocols for sample collection, transport, and analysis, which not only increase costs but also result in a potential for high human error. Furthermore, as these methods are time intensive and are not portable to the site, they are not suited for rapid monitoring. This results in potential feedback delays for treatment strategies which often need swift adjustments.

Detection of cell pigments such as chlorophyll-*a* (Chl-*a*) as a surrogate for algal cells have alleviated some of the aforementioned issues. As Chl-*a* is a fluorescence active pigment, Chl-*a* monitoring *via in situ* fluorescence probes, or through satellite and drone imaging has been used to detect the cells.[12] However, this method also suffers from wide ranging measurement biases and inaccuracies because Chl-*a* is not exclusive to cyanobacteria and can also be found in green algae, diatoms and other aquatic plants. Hence, they do not capture the variations in diversity. Advanced computational models are currently being explored to overcome measurement inaccuracies. Yet, these require complex equipment and are thus expensive.

Electrical characterization of algae

In recent years, there has been a growing interest in electrical techniques for applications in biology. These methods have proven successful in various fields, including medical diagnosis, environmental monitoring, and the analysis and sorting of microbial cells.[13] Their cost-effectiveness, ease of miniaturization, and automation capabilities, makes electrical sensors particularly well-suited for the development of portable tools for on-site cell measurements.[14] Furthermore, their inherently label-free nature positions them as ideal choices for affordable and rapid tools for laboratory experiments focused on cell analysis.

Measurements of electrical cell properties have yielded several applications for algal cell analysis. Notably, electrical impedance based analysis of cell cultures has demonstrated its capacity to discern the difference between cell types due to disparate electrical properties of the cell membrane and cell cytoplasm.[15] Moreover, this method has proven successful in the monitoring of cell culture growth, establishing a correlation between the impedance signal and the growth evolution of the cells.[16]

Electrical techniques are increasingly used for the analysis of single cells. Information about the electrical properties on a single-cell level allows to characterize phenotypic heterogeneity within communities and enables single-cell sorting.[17] Impedance flow cytometry is a commonly used electrical technique for single-cell analysis on algal cells. It has been utilized to discriminate cells by size[18] or viability,[19] measuring changes in intracellular components such as chloroplasts,[20] detecting presence of a cell exoskeleton[21] and the differentiation of algae species.[22] However, the technique measures impedance at only a few, typically two, frequency points which limits the information gathered about the cell's electric properties.

Electrorotation is another technique employed for the analysis of individual cells which provides insights into the electrical properties of single cells across a broad spectrum of frequencies. The technique provides high sensitivity and accuracy over a broad frequency range making it one of the most reliable techniques for measuring electrical properties of cells. However, it is slower than impedance cytometry, measuring a single cell in minutes compared to several hundreds of cells per second for impedance cytometry.[23–25] Applications in the literature concerning algal cells include the evaluation of lipid content,[26,27] monitoring of electro permeabilization phenomena within the cell membrane[28] and the extraction of electrical cell properties, such as membrane capacitance and cytoplasmic conductivity.[29] However, electrorotation is not a full-electric technique and it has limited possibilities for parallelization due to its reliance on a high-speed camera to measure the rotational speed of a cell. Hence electrorotation is a slow technique, not suitable for high throughput cell measurements.

In this paper, a custom designed microfluidic device is used to trap single cells on gold electrodes by positive dielectrophoresis. The fabrication and working principle of the device is described in earlier work.[30] The primary advantage of this system lies in its ability to facilitate single-cell trapping alongside broadband impedance spectroscopy measurements of the individually captured cells. Due to its fully electric operation, the device has a high potential for integration and automation. The detailed broadband impedance measurements enabled by this device are ideally suited for the investigation of electrical properties of different types of algal cells.

Two freshwater species—a green algae, *Chlorella vulgaris*, and a cyanobacteria (blue-green algae), *Microcystis aeruginosa*—are investigated using single-cell broadband impedance spectroscopy. Impedance measurements of single cells of these two species show significant differences in impedance over the entire spectrum. Control experiments verified that these differences are due to the presence of vacuoles in *Microcystis aeruginosa* since the removal of the vacuoles results in a similar spectrum as *Chlorella vulgaris*. These results show for the first time that the presence of vacuoles in *Microcystis aeruginosa* algae can be detected by impedance spectroscopy and used as a discriminative factor to distinguish *Microcystis aeruginosa* from *Chlorella vulgaris*, enabling applications of our system for early detection and discrimination of algal cells. Furthermore, we constructed a model of the cell in finite element simulations to compare the calculated impedance with the measurement results. Fitting the model to the measurements enables the characterization of electrical properties related to cell cytoplasm, wall, and membrane. Our findings open the way towards improved impedance analysis of cytoplasm and cell

membrane properties for fast detection, discrimination, and characterization of cells with applications from laboratory research on algal populations to on-site rapid detection of algae.

Materials and methods

Algal and cyanobacterial cultivation

The freshwater green algae *Chlorella vulgaris* (211-11b SAG, Germany) and the freshwater cyanobacteria *Microcystis aeruginosa* (1450/03 CCAP, UK) were used in all experiments. The green algae and cyanobacteria were cultivated in individual 2 L glass Schott bottles (Schott, UK). The bottles were illuminated with daylight fluorescent tubes that produced a photon flux of 100 μmol m^{-2} s^{-1} at the surface of the bottle (16/8 h light dark cycle). The cell suspension was mixed, and oxygen was purged by bubbling the reactor with 0.2 μm-filtered air (5 L min^{-1}). The culture medium consisted of Wright's cryptophyte (WC) medium. All experiments were conducted with late-exponential growth phase cultures. The green algae had a cell concentration between 8 to 10 × 10^7 cells per mL and the cyanobacteria had a cell concentration between 16 to 19 × 10^6 cells per mL. The cell concentration was determined by cell counting using a haemocytometer and an Olympus SZX10 stereomicroscope (Olympus Scientific, Germany). During EIS measurements, the WC medium was diluted 1 : 3 in deionized water such that the conductivity of the medium approximated 180 μS cm^{-1}.

Collapsing the gas vacuoles in cyanobacteria

To assess the impact of the presence and absence of gas vacuoles on the electrical impedance, experiments were carried out with *Microcystis* cells that had both intact and collapsed gas vacuoles. The gas vacuoles were collapsed by subjecting the cells to high pressure.[31] Briefly, 1 L of the *Microcystis* suspension was pressurized at 500 kPa for 1 h in a pressure vessel (Platypus saturator, Platypus, Australia), subsequently, the vessel was depressurized, and the cell suspension was transferred to a glass jar. *Microcystis* cells with intact gas vacuoles do not settle, they float around which results in a homogenous suspension. To assess if the pressurization collapsed the gas vacuoles, the suspensions of the *Microcystis* was allowed to settle for 30 min. It was verified that pressure treated culture settled on the bottom of the container, while fresh cultures without pressure treatment did not settle.

Microfluidic sensor fabrication

The fabrication of the microfluidic device is identical to the one described in ref. 30 (Fig. 1). Briefly, a 200 nm thick gold layer with a 50 nm titanium adhesion layer was deposited on a glass wafer by sputtering. The layer was patterned by a lift-off process to form gold coplanar electrodes. A 5 μm thick SU-8 layer was patterned over the electrodes as a passivation layer, with openings over the coplanar electrodes. A second layer of 15 μm thick SU-8 was patterned on top to define the microfluidic channel. The channel was sealed by bonding an unstructured PDMS (polydimethylsiloxaan) slab to the top SU-8 layer. The PDMS slab was coated with a layer of APTES (3-aminopropyl triethoxysilane) and bonded to the SU-8 by baking at 150 °C for 1 hour and applying moderate pressure to ensure good contact between the two materials. To increase the sensitivity of the impedance measurements, the gold electrode surface was nanostructured by immersing them in a 100× diluted PBS (phosphate-buffered saline) solution and applying a constant potential of 16 V over the electrodes.[49] The electrode openings were 60 μm × 60 μm in size and were centered over a coplanar electrode pair, with the gap between the electrode pair being 4 μm. The microfluidic channel had a height of 15 μm and a width of 300 μm.

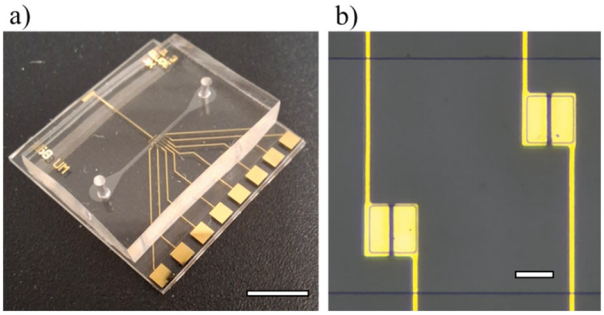

Fig. 1 Microfluidic device images. (a) Photograph of the microfluidic chip (scale = 5 mm). (b) Microscope image of the microfluidic channel with two pairs of gold coplanar sensing electrodes (scale = 50 μm).

Experimental setup

A 250 μL Hamilton glass syringe containing the cell solution was fitted in a syringe pump to inject the cells into the microfluidic channel. The solution was injected at a rate of 20 μL h^{-1}. The "two-voltage" method[30] was employed to ensure that only a single cell was trapped on the electrodes. In brief, cells are drawn to the trap by positive dielectrophoresis when a high voltage, 5 V_{pp} (peak-to-peak voltage) at 5 MHz, is applied. A lower voltage, 1 V_{pp}, maintains the position of the trapped cell without attracting additional cells, enabling precise control over the number of trapped cells. Once a single cell is trapped, the flow in the channel is halted, and the DEP signal is deactivated. The cell's impedance is then measured by connecting the electrodes to an impedance analyzer (Wayne Kerr Precision impedance analyzer 6500B). Impedance Z_{cell} was measured with a 300 mV_{RMS} (root mean square voltage) signal between 100 Hz and 20 MHz. A moving average operation with a window of 10 frequency points was used on the impedance spectra to reduce the noise. After the cell measurement, the cell is released by increasing the flow rate in the microfluidic channel. A reference measurement of the impedance of the empty trap Z_{ref} was taken after release of the cell. The magnitude change $\Delta|Z|$ and phase change $\Delta\varphi$ was then calculated from these measurements using eqn (1) and (2), where $|Z|$ denotes the magnitude of the impedance and φ the phase angle.

$$\Delta|Z| = \frac{|Z|_{\text{cell}} - |Z|_{\text{ref}}}{|Z|_{\text{ref}}} \times 100 \quad (1)$$

$$\Delta\varphi = \varphi_{\text{cell}} - \varphi_{\text{ref}} \quad (2)$$

Simulations

Finite element simulations of impedance spectra were performed in COMSOL Multiphysics using the electric currents interface. A single 60 μm × 60 μm coplanar electrode pair with a cell in the middle of the gap was modeled in the simulation environment. The cell was modeled as a double shelled sphere where the inner core represented the cell cytoplasm, and the outer shell represented the cell wall. The inner shell, representing the cell membrane, consisted of a contact impedance boundary condition. A 1 V AC voltage was applied to one of the electrodes while the second was grounded and this simulation was run for frequencies between 10 Hz and 100 MHz. In the simulations, a parasitic capacitance of 60 fF was added in parallel with the electrodes to model the stray capacitance on the PCB and between the signal cables during the measurement. This value was selected based on the average measured parasitic capacitance.

The electric double layer effect was not modelled in simulations. Therefore, the simulated impedance does not represent the measured impedance at low frequencies. The impedance between the electrode pair was calculated with and without the presence of a cell. The impedance without cell was subtracted from the impedance with cell, using eqn (1) and (2), to assess the impedance change due to cell contribution and compare it with the measured data. The electrical cell parameters were adjusted manually until an optimal fit between the simulated and measured impedance was achieved. From this fitted model, electrical cell properties such as membrane permittivity ε_{mem} and cytoplasm conductivity σ_{cyto} are extracted, enabling a semi-quantitative comparison of cell types based on subcellular electrical properties.

The parameters of the cell model were divided into three categories. Firstly, the fitting parameters are the parameters which were optimized for the model to fit the measurements. Fitting the measurement to the model allows for an estimation of the value of these parameters. The fitting parameters are cytoplasm conductivity, wall conductivity, membrane permittivity and cell radius. In the second category are the fixed parameters which were set based on literature or measurement. These parameters include: wall thickness,[32,33] medium permittivity,[34] medium conductivity (measured), membrane conductivity (assumed non-conductive[35]) and membrane thickness.[36] The final category consists of parameters which did not influence the cell impedance within the measured frequency range. These parameters include cytoplasm permittivity and wall permittivity. Higher frequency measurements are required to extract them from an impedance fit since these parameters influence cell impedance only at frequencies above 10 MHz.

Results

Microscopic imaging of algae

The freshwater green algae *Chlorella vulgaris* and cyanobacteria *Microcystis aeruginosa* were imaged under a microscope at 100× magnification with the aid of immersion oil. *Chlorella vulgaris* is a eukaryotic microalgae species characterized by its relatively larger size, and the presence of distinct chloroplasts and other organelles, which are visible under brightfield microscopy (Fig. 2). In contrast, *Microcystis aeruginosa*, a prokaryotic species, has much smaller cells and does not have a nucleus when compared to eukaryotic species like *Chlorella*. The absence of membrane-bound organelles in *Microcystis* gives it a simpler structure, reflecting the differences between eukaryotic and prokaryotic cell architecture (Fig. 2). Under blue light illumination (430–470 nm), both algae and cyanobacteria fluoresce red due to the presence of chlorophyll pigments, which absorb the blue light and re-emit it in the red region (680–700 nm). Notably, in *Microcystis* cells, the gas vacuoles are visible as dark spots against the red fluorescence because they do not fluoresce. These gas vacuoles are absent in the *Chlorella* cells, which lack such structures, providing a clear distinction between the two species (Fig. 2).

Impedance spectroscopy measurements

In two separate experiments, *Chlorella vulgaris* and *Microcystis aeruginosa* cells respectively were injected into the microfluidic chip and the broadband impedance of trapped single cells was measured. Each cell measurement was subtracted from a reference measurement without cell to achieve a differential impedance output using eqn (1) and (2). In Fig. 3a and b the differential impedance of both cell types is shown.

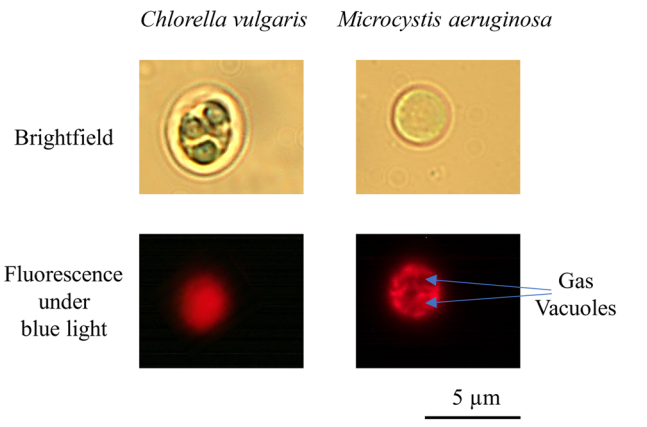

Fig. 2 Cell imaging. Cells of *Microcystis aeruginosa* and *Chlorella vulgaris* imaged under a microscope under brightfield mode and fluorescence under blue light.

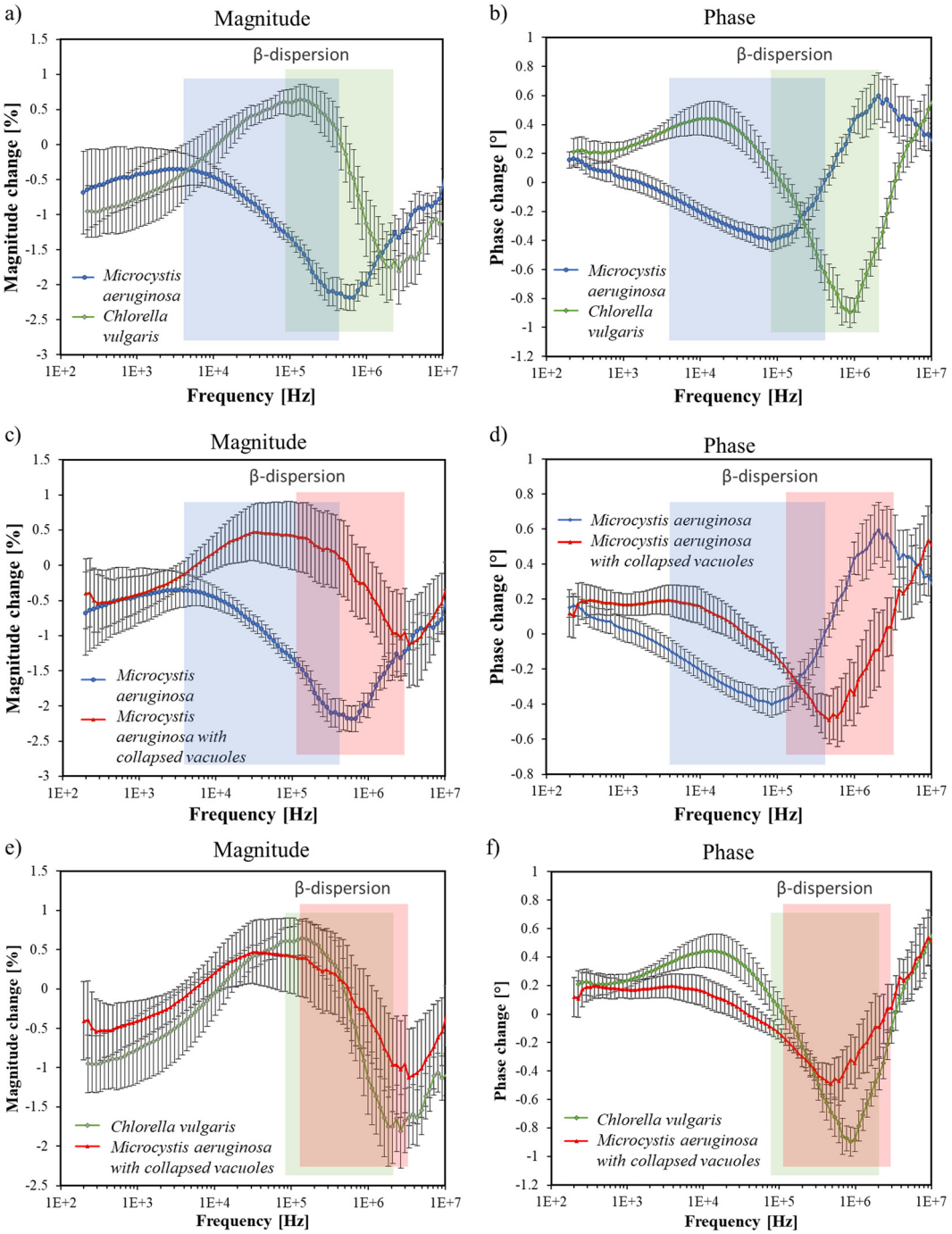

Fig. 3 Impedance spectroscopy measurements of single cells. Average measured magnitude (a, c and e) and phase impedance (b, d and f) change from single-cell algae experiments on three types of cells: *Chlorella vulgaris*, *Microcystis aeruginosa* and *Microcystis aeruginosa* cells after pressure treatment which damaged vacuoles from the cell cytoplasm. (a) and (b) compares *Microcystis aeruginosa* with *Chlorella vulgaris*. (c) and (d) compares regular with pressure treated *Microcystis aeruginosa*. (e) and (f) compares pressure treated *Microcystis aeruginosa* with *Chlorella vulgaris* cells. Sample sizes were 9, 10 and 11 for *Chlorella vulgaris*, *Microcystis aeruginosa* and pressure treated *Microcystis aeruginosa*, respectively. Error bars indicate standard error. β-dispersion frequency region is indicated in the color code of the curves.

Chlorella vulgaris shows a significantly different impedance change compared to *Microcystis aeruginosa* over a broad frequency range. Only at low frequencies, below 10 kHz for the magnitude and below 1 kHz for the phase, the impedance change is similar for both cells. Below these frequencies, the electrical double layer effect at the interface between the gold electrode and the solution dominates the measurement. This largely capacitive impedance masks the contribution of the trapped cell in the measurement; hence any impedance change in this low frequency range can be attributed to the double layer effect.

Chlorella vulgaris showed a 0.5% increase in impedance amplitude at around 100 kHz followed by a −1.5% decrease

around 2 MHz. This impedance signature is common for cells and is related to cell membrane polarization also called β-dispersion.[37] The cell membrane acts as an insulator at lower frequencies, causing an increase in total impedance. At higher frequencies, here above 100 kHz, the electric field starts to penetrate through the cell membrane into the cell cytoplasm. Since the cytoplasm is more conductive than the surrounding medium, a drop in impedance magnitude is observed in the measurements (Fig. 3a green area). The phase data can similarly be explained since the polarization of the capacitive cell membrane causes a more negative phase in the total measured impedance. Starting from 100 kHz the phase angle is negative and reaches a minimum of −1° around 1 MHz. When the electric field penetrates through the membrane, the highly conductive cell cytoplasm causes the total measured impedance to be more resistive rather than capacitive. Hence the phase change increases at higher frequencies crossing zero at around 2 MHz and becomes a positive value (Fig. 3b green area).

Microcystis aeruginosa does not show an increased impedance magnitude around 100 kHz, however, the β-dispersion effect is clearly visible in the measured data (Fig. 3a, b blue area). The impedance magnitude drops down to negative impedance change values and reaches a minimum of −2.3% at 500 kHz. This local minimum is situated at a significantly lower frequency compared to the C*hlorella* cells where the minimum occurred at 2 MHz. A similar observation can be made for the phase data. *Microcystis aeruginosa* does not show an initial increase in phase change. However, the phase drops to a minimum of −0.4° at around 100 kHz from there it increases with frequency, crossing zero at around 500 kHz. Like the magnitude data, this zero crossing occurs at a significantly lower frequency compared to *Chlorella* where it was situated at around 2 MHz. It can be concluded that the β-dispersion effect in the impedance occurred at lower frequencies for *Microcystis aeruginosa* cells compared to *Chlorella vulgaris* cells.

Above the β-dispersion frequency region (>500 kHz for *Microcystis aeruginosa* and >2 MHz for *Chlorella vulgaris*), the cell impedance is mainly determined by the electrical properties of the cytoplasm since the electric field penetrates through the cell membrane.[38] In this frequency range, a significant difference between *Microcystis aeruginosa* and *Chlorella vulgaris* magnitude and phase components is measured which indicates differing electrical properties of the cytoplasm between the two cell types. Particularly, the phase data presents a clear difference in this frequency range. The phase change of *Microcystis aeruginosa* reaches a maximum of +0.6° at around 2 MHz and starts decreasing with frequency (Fig. 3b). This effect has been described in the literature as the high frequency dispersion related to cytoplasm properties.[35] For *Chlorella vulgaris* cells this high frequency dispersion is not yet apparent in the data and likely occurs at frequencies higher than 10 MHz, the highest experimentally measured frequency (Fig. 3b).

Microcystis aeruginosa and *Chlorella vulgaris* are both freshwater microorganisms and can be found in similar environments. However, *Microcystis aeruginosa* is a blue-green algae that produces cyanotoxins that can be harmful for aquatic life and humans when present in high concentration. *Chlorella vulgaris* is a green alga that does not produce these toxins. *Microcystis aeruginosa* has significant biological differences from *Chlorella vulgaris* since it contains small pockets of air inside its cytoplasm called gas vacuoles which allow them to be suspended in still water without settling to the bottom. The gas vacuoles can take up more than half of the volume of the cell and should therefore have an impact on the electrical properties of the cell.[39,40] To assess the effect of vacuoles on the single-cell impedance of *Microcystis aeruginosa*, a culture was cultivated identical to the one in previous experiments. Before the impedance measurement, the vacuoles were collapsed by applying a high pressure to the solution which causes the vacuoles to rupture, releasing the air from the cell cytoplasm. After this pressure treatment which collapsed the gas vacuoles, the *Microcystis aeruginosa* cells were unable to remain suspended in still water but instead sedimented, indicating that the proportion of gas within the cells decreased.

The impedance of *Microcystis aeruginosa* with the collapsed vacuoles differs significantly from the culture with intact vacuoles as is shown in Fig. 3c and d. After the gas vacuoles collapsed, the β-dispersion effect shifted to higher frequencies. In fact, the collapsed cells impedance largely overlaps with that of *Chlorella vulgaris* (Fig. 3e and f). The maxima and minima of impedance change appear at roughly the same frequencies, differing only in amplitude. The higher amplitude is likely due to the larger average cell size of *Chlorella vulgaris* cells compared to *Microcystis aeruginosa* cells.[41] Microscopy measurements indicated that *Chlorella vulgaris* cells had an average radius of 3.5 ± 0.4 μm, while *Microcystis aeruginosa* cells exhibited an average radius of 2.6 ± 0.3 μm. The presence of vacuoles appears to be the main cause of the difference in impedance between *Microcystis aeruginosa* and *Chlorella vulgaris* cells. These results show that impedance measurements could be used to detect the cyanobacteria *Microcystis aeruginosa* and differentiate it from other common freshwater algae based on vacuole content with single-cell resolution.

This finding opens the way to fast and on-site electrical detection of species with gas vacuoles such as *Microcystis aeruginosa*, addressing key limitations of conventional field-based methods. Simple field-based tests, such as the finger and stick tests, rely on the adherence of filamentous algae to a stick or finger and are not suited to distinguishing between unicellular microalgae like *Chlorella vulgaris* and unicellular cyanobacteria like *Microcystis aeruginosa*.[42] The pressure test (also known as jar test or hammer, cork and bottle test) exploits the buoyancy of cyanobacteria with gas vacuoles, which allows them to float to the surface over time, but this approach is slow (often taking several minutes to hours), qualitative, and not readily automated.[43] Unlike conventional

field tests (*e.g.*, finger or jar tests), this method offers the possibility of automation and miniaturisation, opening a pathway for developing real-time, *in situ* detection tools that are cost-effective and scalable. Although this work presents a proof-of-concept, the underlying principle can support broader applications in the future, including the detection of other cellular properties such as lipids, starch or morphological changes under stress conditions.

Simulations and extraction of cell properties

The data in Fig. 3c and d showed that impedance measurements were able to discriminate between *Microcystis aeruginosa* cells with intact and collapsed vacuoles on a single-cell level. However, based on the measurements alone it is not possible to relate the difference in impedance to changes in the electrical properties of the cell. To understand what differences

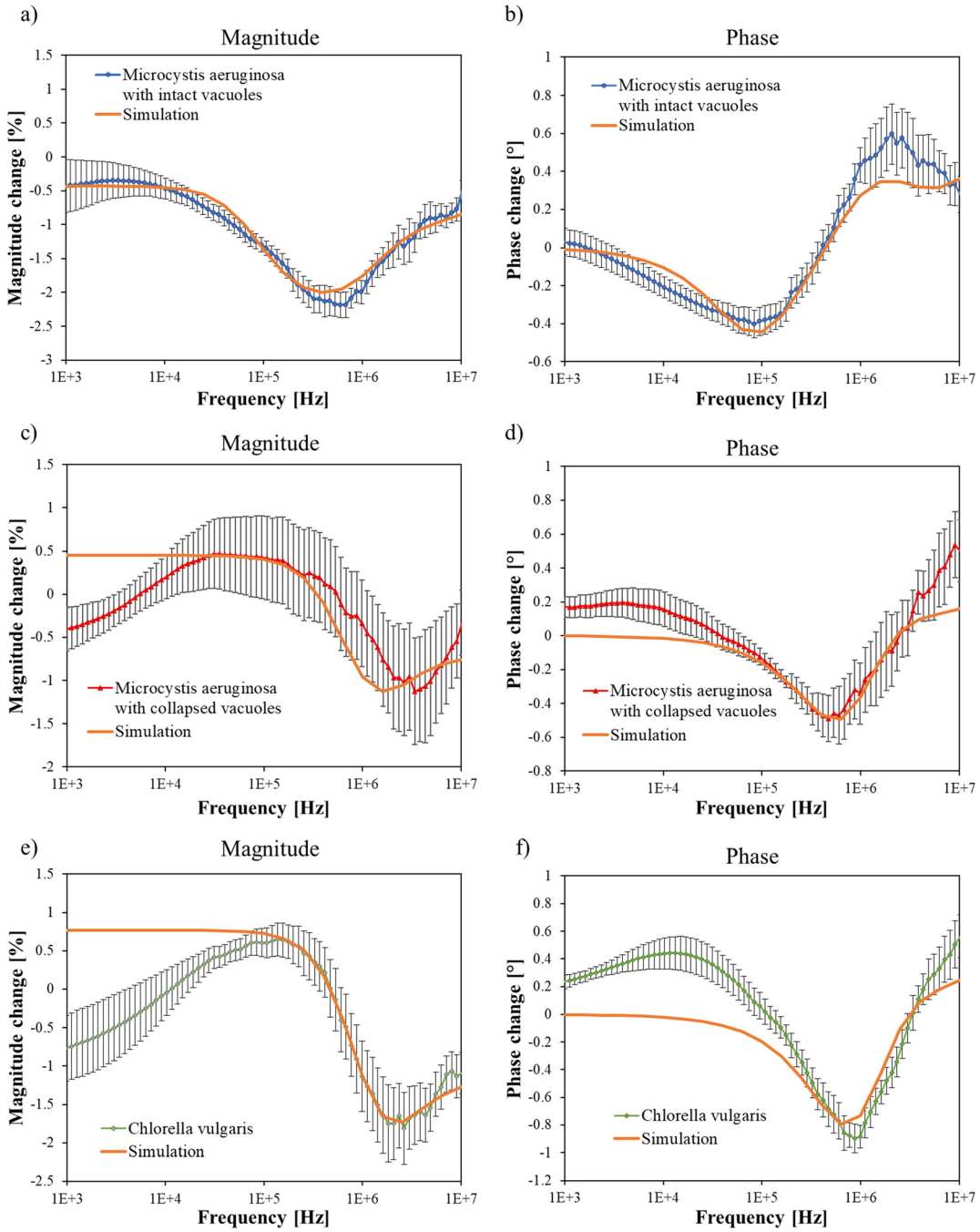

Fig. 4 Simulation of single-cell impedance. Calculated impedance change caused by a single cell between two coplanar electrodes using finite element simulations in COMSOL. The magnitude and phase values of the best fit of the model to the impedance measurements of *Microcystis aeruginosa* with intact (a and b) and collapsed (c and d) vacuoles and of *Chlorella vulgaris* (e and f) are shown together with the measurements. The cell was modelled as a double shelled sphere.

Table 1 Parameters of the COMSOL double shell model. Parameters in bold were varied to optimize the fit to the measurement

	Microcystis aeruginosa	Collapsed *Microcystis aeruginosa*	*Chlorella vulgaris*
Cytoplasm permittivity [F m^{-1}]	$50\varepsilon_0$	$50\varepsilon_0$	$50\varepsilon_0$
Cytoplasm conductivity [S m^{-1}]	0.45	1	0.8
Membrane permittivity [F m^{-1}]	$38\varepsilon_0$	$3.9\varepsilon_0$	$2.1\varepsilon_0$
Membrane conductivity [S m^{-1}]	1×10^{-7}	1×10^{-7}	1×10^{-7}
Wall permittivity [F m^{-1}]	$60\varepsilon_0$	$60\varepsilon_0$	$60\varepsilon_0$
Wall conductivity [S m^{-1}]	1.9	1.3	1.1
Membrane thickness [nm]	8	8	8
Wall thickness [nm]	40	40	40
Cell radius [μm]	3	3	3.7
Medium permittivity [F m^{-1}]	$80\varepsilon_0$	$80\varepsilon_0$	$80\varepsilon_0$
Medium conductivity [S m^{-1}]	1.3×10^{-2}	1.585×10^{-2}	1.79×10^{-2}

in electrical properties lead to changes in impedance measurements, a simplified cell model was constructed in a finite element simulation. The cell model consisted of a double-shelled sphere where the inner core represents the cell cytoplasm and the inner and outer shell represent the cell membrane and wall respectively.[29] Each part of the cell was characterized by its electrical conductivity and permittivity. The cell was then modeled in the environment of the gold electrodes to calculate the measured impedance change caused by the cell. The model included a parasitic capacitance of 60 fF to allow proper fitting to the measured data. In Fig. 4 the best fit of the simulated impedance is shown for *Microcystis aeruginosa* with intact and collapsed vacuoles and for *Chlorella vulgaris*. The corresponding fitting parameters are given in Table 1.

The simulated *Microcystis aeruginosa* with intact vacuoles provides a good fit to the measured data over the entire frequency range, mimicking the general shape of the impedance change for both magnitude and phase components. The simulation remains mostly within the standard deviation of the measurements. Both the simulated *Microcystis aeruginosa* with collapsed vacuoles and *Chlorella vulgaris* showed a mismatch with the measurement at frequencies below 10 kHz. This is due to the double layer effect, present at the interface between the gold electrodes and the solution,[44] which was not considered in the simulations. At higher frequencies, the double layer effect becomes negligible, and simulation falls within the standard deviation of the measurements.

There are three main differences in electrical properties between *Microcystis aeruginosa* and *Chlorella vulgaris* according to the results of the simulations (Table 1). The cytoplasm conductivity parameter of *Microcystis aeruginosa* with intact vacuoles is about half of *Chlorella vulgaris*, 0.45 S m^{-1} and 0.8 S m^{-1}, respectively. The reduced conductivity of the cytoplasm can be attributed to the presence of air in the vacuoles, which can occupy around 50% of the cytoplasm's volume.[39,40] Since air is a poor conductor compared to cytoplasmic fluid, its accumulation within the vacuoles significantly lowers overall cytoplasmic conductivity.

Secondly, the cell wall conductivity is higher (1.9 S m^{-1}) for *Microcystis aeruginosa* compared to 1.1 S m^{-1} for *Chlorella vulgaris* (Table 1). However, it is not straightforward to connect this change in conductivity to biological differences since little is known about how cell wall properties influence their conductivity. Cell walls of cyanobacteria like *Microcystis aeruginosa* predominantly contain peptidoglycan and lipopolysaccharides,[45] while the cell wall of *Chlorella vulgaris* is primarily composed of layers of chitin-like fibers and hemicellulosic material.[32] Additionally, an increase in cell wall conductivity has a similar effect on the impedance as an increase in cell wall thickness. The lower cell wall conductivity observed in *Chlorella vulgaris* could, therefore, also be attributed to a thinner cell wall compared to that of *Microcystis aeruginosa*. In the simulation, the cell wall thickness was set according to values reported in the literature,[32,33] but variations in cell wall thickness can occur depending on the age of the culture and environmental conditions.[46]

Thirdly, the membrane permittivity is significantly higher ($38\varepsilon_0$) for *Microcystis aeruginosa* compared to $2.1\varepsilon_0$ for *Chlorella vulgaris* (Table 1). This difference can be explained by observations in other works where cell membrane properties are influenced by the differences in the character and structural integrity of the cytoplasm.[47] This is further supported by the fact that the membrane permittivity for *Microcystis* with collapsed gas vacuoles ($3.9\varepsilon_0$) was significantly lesser than that of the *Microcystis* cell with intact gas vacuoles (Table 1). The double-shelled sphere model does not explicitly model the vacuoles, they are only implicitly contained in the total properties of the cytoplasm. Further simulations are required with extended models that can take into account vesicle in the cytoplasm such as double-shell model including vesicles (D-S-V model) to assess the effect of vacuoles on the cell impedance.[48]

Finally, the simulated cell radii of *Microcystis aeruginosa* and *Chlorella vulgaris* were 3.0 μm and 3.7 μm, respectively. This relative difference in simulated size is consistent with the actual cell dimensions, as *M. aeruginosa* is known to be smaller than *C. vulgaris*. Microscopy measurements indicated that *C. vulgaris* cells had an average radius of 3.5 ± 0.4 μm, while *M. aeruginosa* cells exhibited an average radius of 2.6 ± 0.3 μm. The higher value in the simulation compared to the actual radius, particularly for *Microcystis* was necessary to achieve an accurate fit with the measured impedance. The parameters in Table 1 should therefore be primarily seen as fitting parameters and not precise quantitative values directly corresponding to biological properties. The model is designed to provide insights

and a framework to understand relative changes in cell characteristics rather than enabling a one-to-one match with actual cell characteristics. Hence the model enables identifying cell properties which cause the differences in impedance between *Microcystis aeruginosa* and *Chlorella vulgaris*. According to the model, the difference in impedance is mainly caused by changes in four cell parameters: cytoplasm conductivity, membrane permittivity, wall conductivity, and cell radius.

Conclusions

In this study, we employed a custom-designed microfluidic chip to isolate individual algal cells and perform broadband impedance spectroscopy. Our measurements revealed a clear distinction in the impedance spectra of *Microcystis aeruginosa* (a cyanobacterium commonly referred to as blue-green algae) and *Chlorella vulgaris* (a green alga). Both species exhibited the characteristic β-dispersion associated with cell membrane polarization. However, *M. aeruginosa* showed this feature at notably lower frequencies compared to *C. vulgaris*. This difference in frequency response enables discrimination between the two species at the single-cell level using impedance spectroscopy.

Control experiments provided insight into the biological origin of this spectral difference. Specifically, we observed that the presence of gas vacuoles in *M. aeruginosa*—air-filled structures within the cytoplasm—contributes significantly to the altered impedance response. When the vacuoles were collapsed, the measured impedance spectrum closely resembled that of *C. vulgaris*, indicating that the vacuoles play a key role in modulating the cell's dielectric properties.

To further understand these findings, we developed a finite element model of the cell based on a double-shelled sphere geometry. By fitting the simulated impedance response to the experimental data, we determined that *M. aeruginosa* cells with intact vacuoles exhibit lower cytoplasmic conductivity, compared to *C. vulgaris* and vacuole-collapsed *M. aeruginosa* cells. This is in line with expectations since the vacuoles are non-conductive. Additionally, *M. aeruginosa* cells with intact vacuoles exhibit a higher membrane permittivity and cell wall conductivity. These results are consistent with prior studies suggesting that the composition and integrity of the cytoplasm can influence membrane and wall properties. However, the presence or absence of vacuoles does not fully explain the observed changes in electrical properties of cell wall and membrane, suggesting the need for more detailed structural models.

Our findings demonstrate that impedance spectroscopy can effectively distinguish *M. aeruginosa* from *C. vulgaris*, highlighting its potential as a rapid, label-free method for detecting harmful algal species in freshwater environments. Our device cannot be directly applied in marine ecosystems as the high conductivity of seawater interferes with the positive dielectrophoretic force which is necessary to trap single cells. Samples from saltwater ecosystems would need to be diluted to reduce the medium conductivity before the cells can be analyzed in our system.

Future research using the device described in this manuscript will investigate other microalgae with diverse sizes and intracellular compositions. Such investigations may broaden the scope of impedance-based diagnostics and pave the way towards the development of portable, high-throughput impedance sensors for identification of bloom-forming species in lakes and ponds.

Data availability

Experimental data related to the single cell measurements depicted in the figures of the manuscript is included as ESI.†

All data is stored on the KU Leuven database.

Further supporting data can be made available upon request to the authors.

Conflicts of interest

There are no conflicts to declare.

Acknowledgements

This work is funded by the Flemish Fund for Scientific Research (FWO G020119N) and (FWO 101029353). We would like to thank Prof. Ilse Smets (KU Leuven) for her input in conceptualizing this work.

References

1 B. Moss, *Ecology of Fresh Waters: A View for the Twenty-First Century*, John Wiley & Sons, 4th edn, 2010.
2 J. A. Thornton, W. R. Harding, M. Dent, R. C. Hart, H. Lin, C. L. Rast, W. Rast, S. O. Ryding and T. M. Slawski, *Lakes Reservoirs*, 2013, **18**, 298–316.
3 H. W. Paerl and V. J. Paul, *Water Res.*, 2012, **46**, 1349–1363.
4 B. Kubickova, P. Babica, K. Hilscherová and L. Šindlerová, *Environ. Sci. Eur.*, 2019, **31**, 1–27.
5 W. W. Carmichael and G. L. Boyer, *Harmful Algae*, 2016, **54**, 194–212.
6 P. M. Glibert, *Mar. Pollut. Bull.*, 2017, **124**, 591–606.
7 S. B. Watson, C. Miller, G. Arhonditsis, G. L. Boyer, W. Carmichael, M. N. Charlton, R. Confesor, D. C. Depew, T. O. Höök, S. A. Ludsin, G. Matisoff, S. P. McElmurry, M. W. Murray, R. Peter Richards, Y. R. Rao, M. M. Steffen and S. W. Wilhelm, *Harmful Algae*, 2016, **56**, 44–66.
8 J. Huisman, G. A. Codd, H. W. Paerl, B. W. Ibelings, J. M. H. Verspagen and P. M. Visser, *Nat. Rev. Microbiol.*, 2018, **16**, 471–483.
9 A. Schaap, T. Rohrlack and Y. Bellouard, *J. Biophotonics*, 2012, **5**, 661–672.
10 M. Gouda, K. Chen, X. Li, Y. Liu and Y. He, *Sens. Actuators, B*, 2021, **329**, 129229.
11 M. Sun, Z. Yang and B. Wawrik, *Front. Plant Sci.*, 2018, **9**, 1–10.
12 D. M. Anderson, *Ocean Coast. Manag.*, 2009, **52**, 342–347.

13 Y. Xu, X. Xie, Y. Duan, L. Wang, Z. Cheng and J. Cheng, *Biosens. Bioelectron.*, 2016, **77**, 824–836.
14 S.-N. Hosseini, P. S. Das, V. K. Lazarjan, G. Gagnon-Turcotte, K. Bouzid and B. Gosselin, *IEEE Trans. Biomed. Circuits Syst.*, 2023, **17**, 202–228.
15 M. R. Jett, M. Z. Rashed, S. P. Hendricks and S. J. Williams, *J. Appl. Phycol.*, 2021, **33**, 1643–1650.
16 M. C. Martínez-Bisbal, N. Carbó Mestre, R. Martínez-Máñez, J. Bauzá and M. Alcañiz Fillol, *Sens. Actuators, B*, 2019, **281**, 44–52.
17 H. Hadady, D. Redelman, S. R. Hiibel and E. J. Geiger, *AIMS Biophys.*, 2016, **3**, 398–414.
18 J. Sui, F. Foflonker, D. Bhattacharya and M. Javanmard, *Sci. Rep.*, 2020, **10**, 1–9.
19 Y. Song, M. Li, J. Yang, J. Wang, X. Pan, Y. Sun and D. Li, *Sens. Actuators, B*, 2014, **194**, 164–172.
20 T. Tang, X. Liu, Y. Yuan, T. Zhang, R. Kiya, K. Suzuki, Y. Tanaka, M. Li, Y. Hosokawa and Y. Yalikun, *Sens. Actuators, B*, 2022, **358**, 131514.
21 D. S. de Bruijn, P. M. ter Braak, D. B. Van de Waal, W. Olthuis and A. van den Berg, *Biosens. Bioelectron.*, 2021, **173**, 112808.
22 G. Benazzi, D. Holmes, T. Sun, M. C. Mowlem and H. Morgan, *IET Nanobiotechnol.*, 2007, **1**, 94–101.
23 E. A. Henslee, *Electrophoresis*, 2020, **41**, 1915–1930.
24 K. Keim, M. Z. Rashed, S. C. Kilchenmann, A. Delattre, A. F. Gonçalves, P. Éry and C. Guiducci, *Electrophoresis*, 2019, **40**, 1830–1838.
25 J. Chen, C. Xue, Y. Zhao, D. Chen, M. H. Wu and J. Wang, *Int. J. Mol. Sci.*, 2015, **16**, 9804–9830.
26 Y. S. Lin, S. Tsang, S. Bensalem, C. C. Tsai, S. J. Chen, C. L. Sun, F. Lopes, B. Le Pioufle and H. Y. Wang, *Biosens. Bioelectron.*, 2021, **173**, 112772.
27 Y. Wu, C. Huang, L. Wang, X. Miao, W. Xing and J. Cheng, *Colloids Surf., A*, 2005, **262**, 57–64.
28 C. I. Trainito, O. Français and B. Le Pioufle, *Electrophoresis*, 2015, **36**, 1115–1122.
29 J. Wang, V. L. Sukhorukov, C. S. Djuzenova, U. Zimmermann, T. Müller and G. Fuhr, *Protoplasma*, 1997, **196**, 123–134.
30 R. Van den Eeckhoudt, A.-S. Christiaens, F. Ceyssens, V. Vangalis, K. J. Verstrepen, N. Boon, F. Tavernier, M. Kraft and I. Taurino, *Lab Chip*, 2023, **23**, 4276–4286.
31 G. Cohen-Bazire, R. Kunisawa and N. Pfennig, *J. Bacteriol.*, 1969, **100**, 1049–1061.
32 P. H. Baudelet, G. Ricochon, M. Linder and L. Muniglia, *Algal Res.*, 2017, **25**, 333–371.
33 Y. Zu, S. Hong, C. Xu, W. Li, S. Chen and J. Li, *Environ. Sci. Pollut. Res.*, 2020, **27**, 42254–42263.
34 C. G. Malmberg and A. A. Maryott, *J. Res. Natl. Bur. Stand.*, 1956, **56**, 1.
35 H. Morgan, T. Sun, D. Holmes, S. Gawad and N. G. Green, *J. Phys. D: Appl. Phys.*, 2007, **40**, 61–70.
36 H. Curtis and N. S. Barnes, *Biology*, Worth publishers, Inc, New York, 5th edn, 1989.
37 H. Morgan, T. Sun, D. Holmes, S. Gawad and N. G. Green, *J. Phys. D: Appl. Phys.*, 2007, **40**, 61–70.
38 S. Gawad, L. Schild and P. Renaud, *Lab Chip*, 2001, **1**, 76–82.
39 H. Lehmann and M. Jost, *Arch. Mikrobiol.*, 1971, **79**, 59–68.
40 M. W. Matthews and S. Bernard, *Biogeosciences*, 2013, **10**, 8139–8157.
41 Z. Zhu, O. Frey, N. Haandbaek, F. Franke, F. Rudolf and A. Hierlemann, *Sci. Rep.*, 2015, **5**, 1–14.
42 Z. Sharip, M. H. Zulkifli and M. N. F. Abdul Wahab, Identification of Toxic Blooms of Cyanobacteria in Freshwater (Lake, Ponds) Habitat, in *Protocols for Cyanobacteria Sampling and Detection of Cyanotoxin*, ed. N. Thajuddin, A. Sankara narayanan and D. Dhanasekaran, Springer, Singapore, 2023, pp. 7–16.
43 H. D. L. Abeynayaka, T. Asaeda, K. Tanaka, K. Atsuzawa, Y. Kaneko, H. Nishda and S. Inada, *Water Supply*, 2016, **16**, 1552–1560.
44 A. Koklu, A. Mansoorifar and A. Beskok, *Anal. Chem.*, 2017, **89**, 12533–12540.
45 U. Jürgens, *FEMS Microbiol. Lett.*, 1989, **65**, 47–51.
46 B. H. J. Yap, S. A. Crawford, R. R. Dagastine, P. J. Scales and G. J. O. Martin, *J. Ind. Microbiol. Biotechnol.*, 2016, **43**, 1671–1680.
47 Y. Peng, Z. Zhang, Y. Kong, Y. Li, Y. Zhou, X. Shi and X. Shi, *Ultrason. Sonochem.*, 2020, **63**, 104909.
48 K. Asami and T. Yamaguchi, *Biophys. J.*, 1992, **63**, 1493–1499.
49 R. Van den Eeckhoudt, N. I. Rusli, B. Sieira, S. Garcia Mayo, S. Hussain, V. Vangalis, D. Seveno, K. J. Verstrepen, J. Ustarroz, F. Tavernier, M. Kraft and I. Taurino, *ACS Appl. Electron. Mater.*, 2025, **7**, 3786–3794.

